AIP | Journal of Applied Physics

Structural and band alignment properties of Al2O3 on epitaxial Ge grown on (100), (110), and (111)A GaAs substrates by molecular beam epitaxy

M. K. Hudait, Y. Zhu, D. Maurya, S. Priya, P. K. Patra et al.

Citation: J. Appl. Phys. **113**, 134311 (2013); doi: 10.1063/1.4799367
View online: http://dx.doi.org/10.1063/1.4799367
View Table of Contents: http://jap.aip.org/resource/1/JAPIAU/v113/i13
Published by the American Institute of Physics.

Additional information on J. Appl. Phys.

Journal Homepage: http://jap.aip.org/
Journal Information: http://jap.aip.org/about/about_the_journal
Top downloads: http://jap.aip.org/features/most_downloaded
Information for Authors: http://jap.aip.org/authors

ADVERTISEMENT

JOURNAL OF APPLIED PHYSICS **113**, 134311 (2013)

Structural and band alignment properties of Al_2O_3 on epitaxial Ge grown on (100), (110), and (111)A GaAs substrates by molecular beam epitaxy

M. K. Hudait,[1,a)] Y. Zhu,[1] D. Maurya,[2] S. Priya,[2] P. K. Patra,[3] A. W. K. Ma,[4] A. Aphale,[5] and I. Macwan[5]

[1]*Advanced Devices and Sustainable Energy Laboratory (ADSEL), Bradley Department of Electrical and Computer Engineering, Virginia Tech, Blacksburg, Virginia 24061, USA*
[2]*Center for Energy Harvesting Materials and Systems (CEHMS), Virginia Tech, Blacksburg, Virginia 24061, USA*
[3]*Department of Biomedical Engineering and Department of Mechanical Engineering, University of Bridgeport, Bridgeport, Connecticut 06604, USA*
[4]*Department of Chemical and Biomolecular Engineering and Institute of Materials Science, University of Connecticut, Storrs, Connecticut 06269, USA*
[5]*Department of Electrical and Computer Engineering, University of Bridgeport, Bridgeport, Connecticut 06604, USA*

(Received 24 December 2012; accepted 19 March 2013; published online 5 April 2013)

Structural and band alignment properties of atomic layer Al_2O_3 oxide film deposited on crystallographically oriented epitaxial Ge grown *in-situ* on (100), (110), and (111)A GaAs substrates using two separate molecular beam epitaxy chambers were investigated using cross-sectional transmission microscopy (TEM) and x-ray photoelectron spectroscopy (XPS). High-resolution triple axis x-ray measurement demonstrated pseudomorphic and high-quality Ge epitaxial layer on crystallographically oriented GaAs substrates. The cross-sectional TEM exhibited a sharp interface between the Ge epilayer and each orientation of the GaAs substrate as well as the Al_2O_3 film and the Ge epilayer. The extracted valence band offset, ΔE_v, values of Al_2O_3 relative to (100), (110), and (111) Ge orientations using XPS measurement were 3.17 eV, 3.34 eV, and 3.10 eV, respectively. Using XPS data, variations in ΔE_v related to the crystallographic orientation were $\Delta E_V(110)\text{Ge} > \Delta E_V(100)\text{Ge} \geq \Delta E_V(111)\text{Ge}$ and the conduction band offset, ΔE_c, related to the crystallographic orientation was $\Delta E_c(111)\text{Ge} > \Delta E_c(110)\text{Ge} > \Delta E_c(100)\text{Ge}$ using the measured ΔE_v, bandgap of Al_2O_3 in each orientation, and well-known Ge bandgap of 0.67 eV. These band offset parameters are important for future application of Ge-based p- and n-channel metal-oxide field-effect transistor design. © *2013 American Institute of Physics*.
[http://dx.doi.org/10.1063/1.4799367]

I. INTRODUCTION

With continued scaling of Si complementary metal-oxide semiconductor (CMOS) technology, high mobility III-V and Ge channel materials and device architectures, in addition to metal gate/high-κ gate dielectric and multi-gate transistor configuration, are needed for transistor miniaturization and to enhance transistor performance.[1] Recently, III-V compound semiconductors, namely, InGaAs, InAs, InSb, and InAsSb,[2–8] coupled with high-κ gate dielectrics have been investigated for n-channel field-effect transistors. However, the demonstration of equivalent high-performance p-channel transistor is mandatory to realize energy-efficient CMOS logic. One enticing approach is to replace the Si channel with high intrinsic hole mobility Ge for p-channel device compared to III-V p-channel material.[8–10] Alternative approaches are different surface orientations to improve the carrier mobility,[11–14] strain engineering,[11,15,16] device architecture,[8,9,17] and optimal channel direction.[19–23] Research efforts are currently devoted towards investigation of the Ge as channel material, since higher intrinsic carrier mobility of Ge can provide a larger drive current, and its smaller bandgap can enable operation at a lower voltages. In addition, high-κ dielectrics on Ge are essential to reduce the gate leakage current for low-power operation. Thus, a combination of high-κ dielectric with high mobility Ge provides an opportunity for interface engineering and tailoring transistor performance.

Very recently, it has been demonstrated that the carrier mobility of Ge metal-oxide semiconductor field-effect transistors (MOSFETs) can be enhanced by utilizing a Ge channel with different orientations; the transistors fabricated on (111)Ge substrates exhibited higher electron mobilities (μ_n) of ~1100 cm^2/Vs (Ref. 24) and the hole mobilities (μ_h) of ~650 cm^2/Vs were higher on (110)Ge substrate along ⟨110⟩ direction.[16] The μ_n of Ge with (111) orientation is 1.8× higher than that of (100) and (110) orientations.[18] Moreover, the reported μ_h of (110) Ge channel, orientation along the ⟨110⟩ direction, exhibited 2.3× higher μ_h compared with the (100) Ge.[19] Thus, Ge CMOS with high-κ gate dielectrics is very attractive as one of the post-Si device options with higher-performance and low-power operation. However, finding a *common high-κ gate dielectric* on off-oriented Ge substrates, in order to achieve superior-quality interface between the Ge epitaxial layer and the dielectric film, is a major challenge. The surface orientation also affects the transport properties of

[a)]Tel.: (540) 231-6663. Fax: (540) 231-3362. E-mail: mantu.hudait@vt.edu

 © 2013 American Institute of Physics

the Ge metal-oxide semiconductor (MOS) inversion layer,[25] similar to the case of Si MOSFETs.[25] Furthermore, the interface quality depends on the surface orientations and in a particular orientation, there may be no interfacial layer present between the Ge and the dielectric layer.

Significant research on the high-κ gate dielectrics HfO_2,[26,27] ZrO_2,[28] Al_2O_3,[29,30] Y_2O_3,[31] Lu_2O_3,[32] CeO_2,[33] rare-earth oxides,[34] as well as germanium-oxynitride[35] on the (100)Ge MOS devices has been conducted, with the possibility that integration of these high-κ dielectrics with (100)Ge will allow continued scaling of transistors. Although excellent device performances were achieved using high-κ gate dielectrics on (100)Ge and oxide/(100)Ge band alignment properties, however, little attention has been devoted on the integration of high-κ gate dielectrics on the (110)Ge and (111)Ge and the associated energy band alignment at each interface. High-quality dielectric on (100)Ge, (110)Ge, and (111)Ge interface is essential to eliminate the formation of high density of intrinsic defects with energy levels in the semiconductor band gap[36] due to poor quality native oxides, resulting in Fermi level pinning[37] at the oxide-semiconductor interface. Furthermore, the selected high-κ material should have a valence and conduction band discontinuity larger than 1 eV relative to the Ge channel material[38] to act as a barrier for both holes and electrons. Hence, one purpose of this article is to investigate and compare the band alignment properties between the atomic layer deposited Al_2O_3 oxide film and the crystallographic oriented epitaxial Ge films grown on (100)GaAs, (110)GaAs, and (111)A GaAs substrates using molecular beam epitaxy (MBE) by x-ray photoelectron spectroscopy (XPS) measurement. An additional motivating factor for this study stems from the use of Ge orientations for the device applications as well as Ge surface orientation on interface properties. Thus, the results from this experimental findings are the initial step towards achieving high-performance devices on (110)GaAs for p-channel and on (111)A GaAs for n-channel Ge MOSFET, respectively.

II. EXPERIMENTAL

The undoped epitaxial 60–80 nm thick Ge layers were grown by *in-situ* growth process on (100), (110), and (111)A epi-ready GaAs substrates using separate solid source MBE growth chambers for Ge and III-V materials, connected *via* ultra-high vacuum transfer chamber. Substrate oxide desorption was done at ~680 °C for (100)/6°-oriented GaAs, ~580 °C for (110)-oriented GaAs, and ~550 °C for (111)A-oriented GaAs substrates under an arsenic overpressure of $\sim 1 \times 10^{-5}$ Torr in a III-V MBE chamber. During the substrate oxide desorption, GaAs layer growth, and Ge layer after growth, reflection high energy electron diffraction patterns were recorded for each step of the growth process. An initial 0.2 μm thick undoped GaAs buffer layer was then deposited on each GaAs substrate to generate a smooth surface under a stabilized As_2 flux prior to transferring each GaAs wafer to the Ge MBE chamber for Ge epilayer growth. The details of the growth procedure can be found elsewhere.[39,40]

The 1 nm and 10 nm Al_2O_3 films were grown by atomic layer deposition (ALD) in a Cambridge NanoTech system on epitaxial (100)Ge, (110)Ge, and (111)Ge films using a trimethylaluminum compound as Al precursor and H_2O as the oxygen source. All three oriented Ge epitaxial layers were placed in each run for Al_2O_3 deposition. During the Al_2O_3 growth, the surface temperature of Ge epilayers was kept constant at 250 °C and the Al precursor was kept at room temperature. All Ge epilayers were wet etched to ~5 nm using NH_4OH:H_2O_2:H_2O (2:1:200 volume ratio) for 5 s prior to loading in ALD chamber for Al_2O_3 deposition. Cross-sectional transmission electron microscopy (TEM) was used to characterize the interface between the high-κ dielectric and the crystallographically oriented Ge epilayers. The band alignment of Al_2O_3/(100)Ge, Al_2O_3/(110)Ge, and Al_2O_3/(111)Ge structures was investigated using a PHI Quantera SXM XPS system with a monochromated Al-$K\alpha$ (energy of 1486.7 eV) x-ray source. The Ge 3d and Al 2p core level (CL) binding energy spectra as well as Ge and Al valence band (VB) binding energy spectra for all orientations were collected with a pass energy of 26 eV and an exit angle of 45°. The CL energy position was defined to be the center of the peak width at the half of the peak height (i.e., full width at half maximum). The bandgap of the Al_2O_3 film, the core level, and valence electrons emitted from each film determined from the XPS measurement will allow to determine the valence band offset, ΔE_v, of Al_2O_3 relative to the (100), (110), and (111)Ge films by the method described in Ref. 41. An angle integrated photoelectron energy distribution curves for the valence band maximum (VBM) and the Ge 3d, Al 2p core levels spectra were recorded. The binding energy was corrected by adjusting the carbon 1s CL peak position to 285.0 eV for each sample surface. The ΔE_v and conduction band offset, ΔE_c, is an important parameter to confine the carrier inside of the Ge channel, and recently, we have demonstrated these offsets between the Ge and off-oriented GaAs heterointerfaces. This work provides a comprehensive study on the band alignment properties of the Al_2O_3/Ge system along with the offset values of Ge on off-oriented GaAs substrates.

III. RESULTS AND DISCUSSION

A. Strain relaxation properties of Ge

To determine the structural quality and the relaxation state of Ge epitaxial layers on crystallographic GaAs substrates, high-resolution triple axis x-ray reciprocal space maps (RSMs) were recorded. The relaxation state of Ge layer was obtained from symmetric (004) and asymmetric (115) reflections of RSMs. Figures 1(a) and 1(b) show the RSMs for (004) and (115) reflections obtained from epitaxial Ge grown on (100)6° GaAs substrate. The RSMs exhibit 2 distinct reciprocal lattice point (RLP) maxima and the peak assignments corresponding to those RLP maxima are from (i) the GaAs substrate and (ii) the Ge epilayer. Similarly, Figures 2 and 3 show RSMs of Ge layers grown on (110) and (111)A GaAs substrates, respectively. One can find from these RSMs that the thickness of the fringes now becomes contours of intensity. From these RSMs, one can determine the lattice parameter in the out-of-plane (growth direction), $a_\perp$ (from the symmetric 004 reflection), and the lattice parameter in the growth plane, $a_\parallel$ (from the asymmetric 115 reflection). The degree of relaxation of the Ge layer in each orientation can be calculated from measured lattice

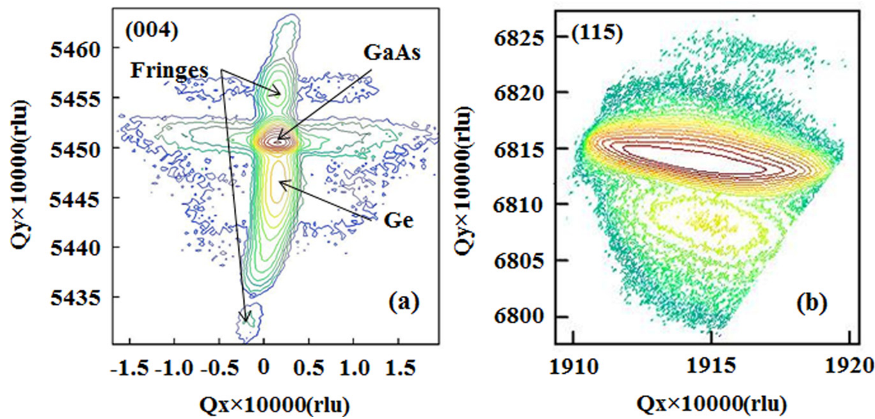

FIG. 1. (a) Symmetric (004) and (b) asymmetric (115) reciprocal space maps of 80 nm Ge/(100)GaAs (6° offcut towards [110] direction) heterostructure. The RSMs are plotted in reciprocal space coordinates and each epilayer peak corresponding to reciprocal lattice point is indicated in this figure.

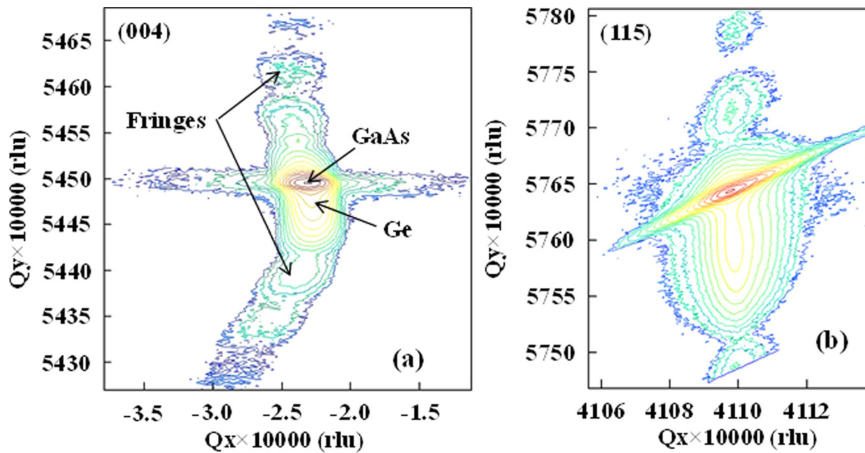

FIG. 2. (a) Symmetric (004) and (b) asymmetric (115) RSMs of 60 nm Ge/(110)GaAs heterostructure. The RSMs are plotted in reciprocal space coordinates and each epilayer peak corresponding to reciprocal lattice point is indicated in this figure.

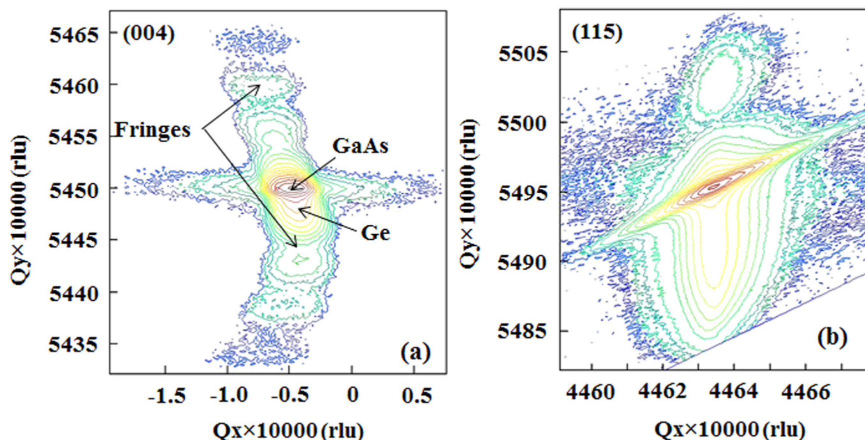

FIG. 3. (a) Symmetric (004) and (b) asymmetric (115) RSMs of 60 nm Ge/(111)A GaAs heterostructure. The RSMs are plotted in reciprocal space coordinates and each epilayer peak corresponding to reciprocal lattice point is indicated in this figure.

parameters and the Poisson's ratio with respect to GaAs substrate. With this information, the degree of relaxation of the Ge layer was limited to only 5%, which is expected since the critical layer thickness of Ge is about 1.8 μm. The minimal relaxation and the thickness fringes indicate the presence of abrupt heterointerface between the Ge layer and the GaAs substrate, which can be also seen from cross-sectional TEM micrographs.

B. Cross-sectional TEM studies of epitaxial Ge on GaAs and Al_2O_3 on epitaxial (110)Ge

Figure 4 compares the high-resolution cross-sectional TEM micrographs of epitaxial Ge grown on (a) (100)/6°GaAs, (b) (110)GaAs, and (c) (111)A GaAs substrates, respectively. There are no threading dislocations observed in this structure, as expected since the lattice mismatch between the Ge epilayer and the GaAs substrate is limited to only 0.07%. The black spot is due to the artifact during the sample preparation. One can find from this figure that it is possible to grow an abrupt Ge/GaAs heterointerface using MBE. Figure 5 shows the cross-sectional TEM micrograph of Al_2O_3 layer deposited on (110)Ge. The Al_2O_3 thickness measured by TEM is ~10 nm, consistent with the ALD deposited thickness. The thickness of the interfacial oxide layer, consisting of a mixture of GeO and GeO_2, as reported by several researchers,[42] was not observed at this TEM magnification

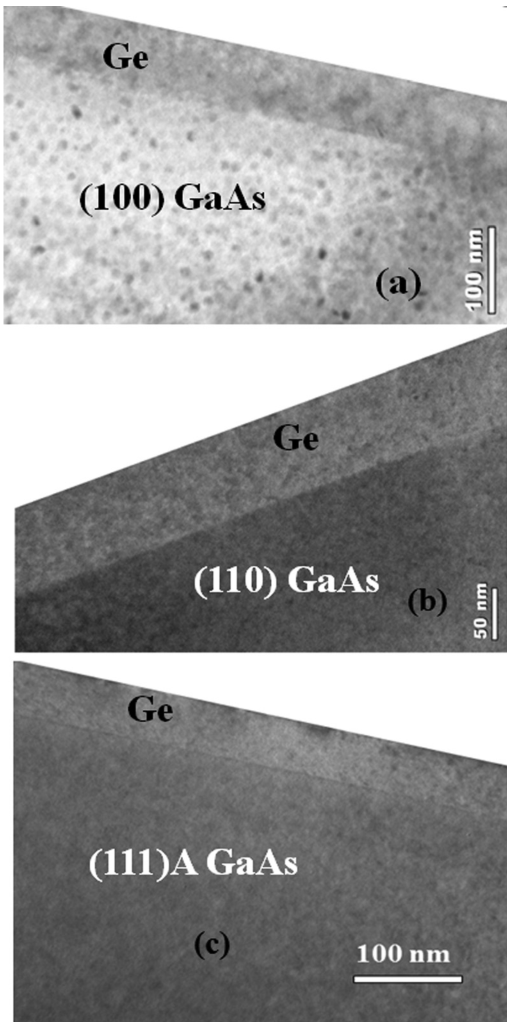

FIG. 4. Cross-sectional TEM micrograph of epitaxial Ge grown on (a) (100)/6°GaAs, (b) (110) GaAs, and (c) (111)A GaAs substrates. The sharp interface between Ge and GaAs was achieved in each orientation.

scale. On one hand, the lower dielectric constant of GeO_2 ($\kappa = 3.0$–3.8)[42] as well as poor chemical and thermal stability, removal of this unwanted layer is essential. The elimination of this poor quality and unstable oxide layer is essential for better electrical transport characteristics namely, equivalent oxide layer thickness, interface states, capacitance-voltage hysteresis, and frequency dispersion. On the other hand, the relatively unstable nature of Ge oxide implies that the removal of unwanted interfacial oxide can be easily achieved and thus represent a potential advantage for high-κ/Ge system.[42] Moreover, the band alignment of the Al_2O_3/(100)Ge interface is not affected by the presence of this thin interfacial layer at room temperature and only post deposition annealing could affect the band alignment due to the formation of thick GeO_2 layer at the oxide and Ge heterointerface.[42]

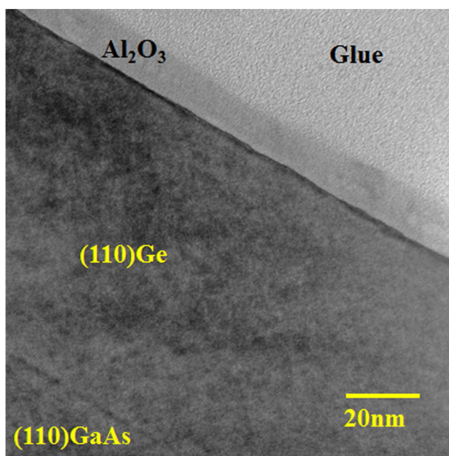

FIG. 5. Cross-sectional TEM micrograph of Al_2O_3 layer deposited on epitaxial (110)Ge layer of structure shown in Figure 4(b).

C. Band alignment properties of Al_2O_3/Ge heterostructures

The valence band offset, ΔE_v, of 3.3 ± 0.1 eV between the Al_2O_3 and the (100)Ge has been studied by several researchers using different deposition methods of Al_2O_3.[43] However, the experimental band offset values on the (110)Ge and (111)Ge epitaxial layers would provide a better insight into the electrical transport properties of the MOS capacitors for p-channel and n-channel MOSFET applications. The value of ΔE_C varying from 2.3 to 2.6 eV can be found in the literature and the reason is partly due to the measurement errors associated with the bandgap of Al_2O_3 layer. These band discontinuities play a crucial role in the electrical transport properties of a MOSFET device. Very recently, we have demonstrated the band offset of GaAs/Ge/GaAs heterostructure and the band offset was indeed dependent on the surface orientations and the order of deposition.[40] In fact, it has been reported that band offsets of two semiconductors can depend on substrate orientation, overlayer crystallinity, surface reconstruction, deposition temperature, deposition rate, microscopic interface dipole, and interdiffusion or reactivity.[44] Therefore, the energy band alignment at the high-κ and crystallographic Ge interface is of great importance, since the sufficient barriers for electron and hole are needed to suppress the tunneling leakage current. Also, the reported hole mobility is higher on (110)Ge and electron mobility on (111)Ge, thus, the measured ΔE_v and ΔE_c values of Al_2O_3 relative to (110)Ge and (111)Ge will provide further insights into the predicted electrical transport mechanisms in the predefined Ge channel layer thickness grown on a large bandgap GaAs barrier layer.

1. Al_2O_3/(100)Ge heterointerface

In order to determine the band offset at the Al_2O_3/(100) Ge heterointerface, XPS spectra were recorded from the following 3 samples: (i) (100) Ge epitaxial layer, (ii) 10 nm thick Al_2O_3 film on (100) Ge, and (iii) interface of 1 nm Al_2O_3 on (100) Ge layer. Figures 6(a) and 6(b) show the Ge 3d CL (E^{Ge}_{Ge3d}) spectrum and VBM (E^{Ge}_{VBM}) of (100) Ge film as well as Al 2p CL (E^{Al}_{Al2p}) spectrum and VBM (E^{Al}_{VBM}) of 10 nm Al_2O_3 film, respectively. Figure 7(a) shows the Ge 3d CL (E^{Ge}_{Ge3d}) and Al 2p CL (E^{Al}_{Al2p}) spectrum of 1 nm Al_2O_3 on (100) Ge interface, respectively. The ΔE_v at Al_2O_3/(100) Ge interface was determined with the following equation[41] using measured CL spectra:

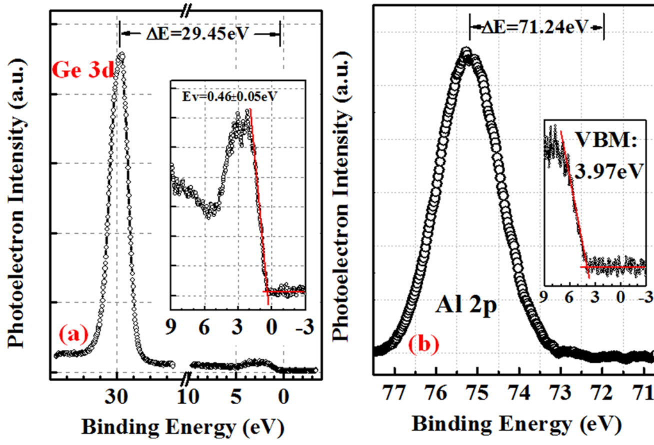

FIG. 6. XPS spectra of (a) Ge 3d core level (E^{Ge}_{Ge3d}) and valence band maximum, VBM (E^{Ge}_{VBM}) of (100) Ge film; (b) Al 2p core level (E^{Al}_{Al2p})spectrum and VBM (E^{Al}_{VBM}) of 10 nm Al_2O_3 film, respectively.

$$\Delta E_V = (E^{Ge}_{Ge3d} - E^{Ge}_{VBM})^{Ge} - (E^{Al}_{Al2p} - E^{Al}_{VBM})^{10nmAl_2O_3} - (E^{Ge}_{Ge3d} - E^{Al}_{Al2p})^{1nmAl_2O_3/Ge\ interface}. \quad (1)$$

Finally, the ΔE_c at Al_2O_3/(100) Ge interface is determined from the following equation:

$$\Delta E_C = E_g^{Al_2O_3} - E_g^{Ge} - \Delta E_V, \quad (2)$$

where $E_g^{Al_2O_3}$ and E_g^{Ge} are the bandgaps of Al_2O_3 determined from Fig. 7(b) and Ge, respectively.

The position of the Ge 3d peak centroid from the XPS measurement was found to be 30.05 ± 0.05 eV as shown in Fig. 6(a). The error bar we defined in this paper is due to the scatter of VB spectra during the fitting of VBM position and considering the linearity and stability of the energy scale of the XPS binding energy spectrum. This value was obtained by measuring the center of the peak width at half of the peak height after Shirley background subtraction. The VBM values are determined by linear extrapolation of the leading edge to the base line of the VB spectra recorded on the bulk Al_2O_3 and thick Ge film to the base lines. Truly, the VBM value is sensitive to the choice of points on the leading edge used to obtain the regression line.[45,46] Several different sets of points were selected over the linear region of the leading edge to perform regressions, and the uncertainty of ΔE_v and ΔE_c values were found to be in the range of 0.05–0.1 eV in the present work. Figure 6(a) shows the VBM for the (100)Ge film. The energy difference between the Ge 3d centroid and the (100)Ge VBM was measured to be 29.45 ± 0.05 eV. Similarly, the energy difference between the Al 2p centroid and the VBM was found to be 71.24 ± 0.05 eV for the 10 nm thick Al_2O_3 film. For the 1 nm Al_2O_3 film on (100)Ge, the energy difference between the Ge 3d centroid and the Al 2p core lines was determined to be 44.96 eV. Using these measured data and Eq. (1), the measured value of ΔE_v for the Al_2O_3/(100) Ge interface is 3.17 ± 0.05 eV. In order to determine the ΔE_c for the Al_2O_3 on (100)Ge, the precise determination of the bandgap of Al_2O_3 is essential. Figure 7(b) shows the O1s CL spectrum of 10 nm Al_2O_3 film and the band gap is determined to be 6.5 ± 0.05 eV. The ΔE_C can be calculated based on the measured ΔE_V and the difference in bandgap of Al_2O_3 and Ge, where $\Delta E_g = \Delta E_V + \Delta E_C$. Using the Eq. (2), the bandgap of Ge 0.67eV, the measured value of ΔE_v, and the measured bandgap of Al_2O_3, the ΔE_C is calculated to be 2.66 ± 0.1eV. These offset values are similar to those obtained by several researchers on ALD Al_2O_3/(100)Ge interface.[43] These results also suggest that the barrier height of Al_2O_3/(100)Ge is enough to obtain low leakage current using Al_2O_3 as high-κ gate dielectrics on (100)Ge. Table I shows the CL to VBM binding-energy difference and resulting band offsets on (100)Ge epitaxial layer. Once we validate the experimental band offset results on epitaxial (100)Ge layer, the similar approach was utilized to determine the band offsets on Al_2O_3/(110)Ge and Al_2O_3/(111)Ge heterointerface.

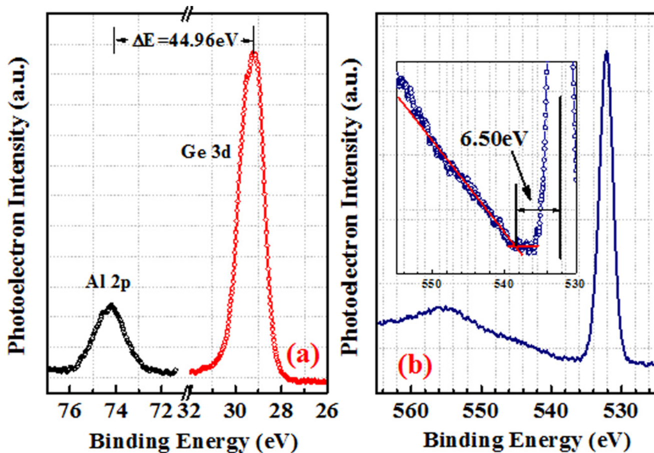

FIG. 7. XPS spectra of (a) Ge 3d (E^{Ge}_{Ge3d}) and Al 2p core level (E^{Al}_{Al2p}) spectra of 1 nm thin Al_2O_3 film/(100)Ge interface, and (b) shows the core level spectrum of 10 nm Al_2O_3 film. The band gap of Al_2O_3 was determined to be 6.5 ± 0.05 eV.

2. Al_2O_3/(110)Ge heterointerface

It has been suggested that the (110)Ge orientation has a significant effect on the enhancement of hole mobility and that has a technological importance, as discussed earlier. The ΔE_V and ΔE_c discontinuities at the Al_2O_3 and (110)Ge heterointerface have been measured using Eqs. (1) and (2). Figures 8(a) and 8(b) show the Ge 3d CL spectrum and

TABLE I. Core-level to VBM binding-energy difference for Al_2O_3 and epitaxial (100)Ge grown on (100)/6° GaAs substrate.

Material and interface	Binding energy difference	Measured band offsets of Al_2O_3/(100)Ge	
		ΔE_V (eV)	ΔE_C (eV)
Ge	$E^{Ge}_{Ge3d} - E^{Ge}_{VBM} = 29.45 \pm 0.05$ eV		
10 nm Al_2O_3	$E^{Al}_{Al2p} - E^{Al}_{VBM} = 71.24 \pm 0.05$ eV		
1 nm Al_2O_3 on Ge	$E^{Al}_{Al2p} - E^{Ge}_{Ge3d} = 44.96$ eV		
E_g of Al_2O_3	6.5 ± 0.05 eV	3.17 ± 0.05	2.66 ± 0.1

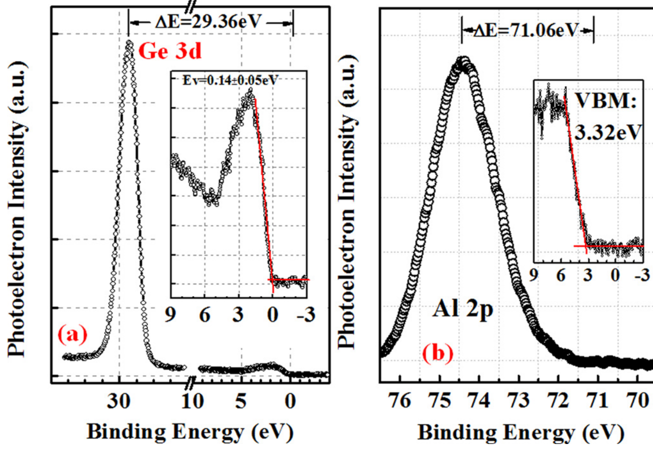

FIG. 8. XPS spectra of (a) Ge 3d core level (E^{Ge}_{Ge3d}) and valence band maximum, VBM (E^{Ge}_{VBM}) of (110)Ge film; (b) Al 2p core level (E^{Al}_{Al2p}) spectrum and VBM (E^{Al}_{VBM}) of 10 nm Al_2O_3 film, respectively.

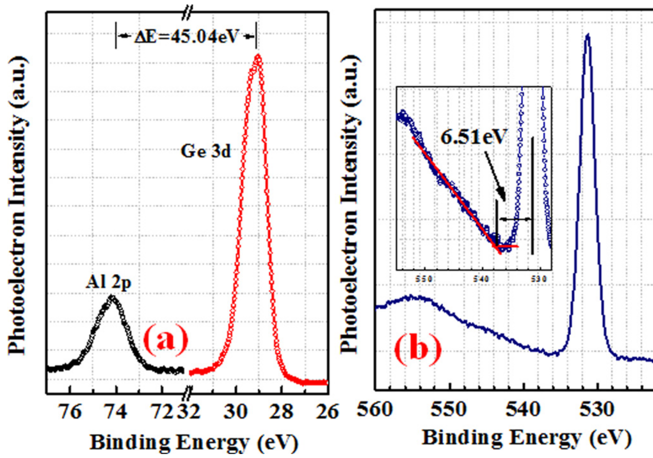

FIG. 9. XPS spectra of (a) Ge 3d (E^{Ge}_{Ge3d}) and Al 2p core level (E^{Al}_{Al2p}) spectra of 1 nm thin Al_2O_3 film/(110)Ge interface, and (b) the CL spectrum of 10 nm Al_2O_3 film. The band gap of Al_2O_3 was determined to be 6.51 ± 0.05 eV.

VBM of (110)Ge film as well as Al 2p CL spectrum and VBM of 10 nm Al_2O_3 film, respectively. Figure 9(a) shows the Ge 3d CL and Al 2p CL spectrum of 1 nm Al_2O_3 on (110)Ge interface, respectively. Figure 9(b) shows the CL spectrum of 10 nm Al_2O_3 film and the band gap is determined to be 6.51 ± 0.05 eV. The measured values of ΔE_v and ΔE_c at the Al_2O_3 on (110)Ge are 3.34 ± 0.05 eV and 2.50 ± 0.1eV, respectively, thus have a potential advantage for hole confinement. The band offset parameters obtained from Al_2O_3/(110)Ge heterointerface is presented in Table II.

3. Al_2O_3/(111)Ge heterointerface

Figures 10 and 11 show the CL XPS spectra for the (111)Ge epitaxial layer, 10 nm Al_2O_3, 1 nm Al_2O_3 on (111)Ge interface, and Al_2O_3 bandgap, respectively. The result obtained from analysis of this data are presented in Table III. The measured values of ΔE_v and ΔE_C for the Al_2O_3 on (111)Ge are 3.1 ± 0.05eV and 2.83 ± 0.1eV, respectively. Although the magnitude of the variation of the ΔE_v and ΔE_c is consistent to the values on (100)Ge

TABLE II. Core-level to VBM binding-energy difference for Al_2O_3 and epitaxial (110)Ge grown on (110)GaAs substrate.

Material and interface	Binding energy difference	Measured band offsets of Al_2O_3/(100)Ge	
		ΔE_V (eV)	ΔE_C (eV)
Ge	$E^{Ge}_{Ge3d} - E^{Ge}_{VBM} = 29.36 \pm 0.05$ eV		
10 nm Al_2O_3	$E^{Al}_{Al2p} - E^{Al}_{VBM} = 71.06 \pm 0.05$ eV		
1 nm Al_2O_3 on Ge	$E^{Al}_{Al2p} - E^{Ge}_{Ge3d} = 45.04$ eV		
E_g of Al_2O_3	6.51 ± 0.05 eV	3.34 ± 0.05	2.50 ± 0.1

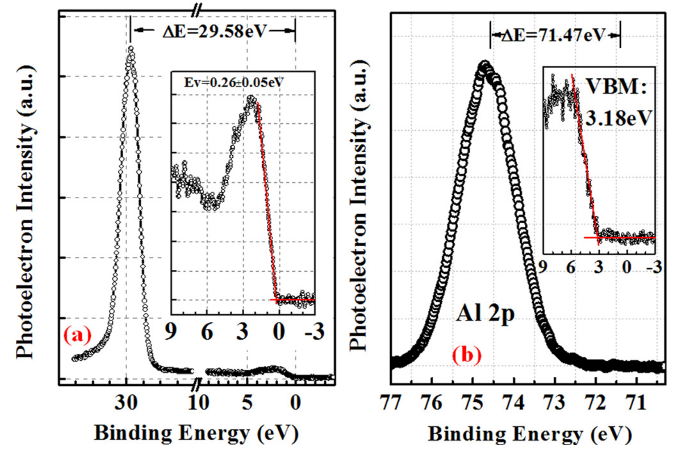

FIG. 10. XPS spectra of (a) Ge 3d core level (E^{Ge}_{Ge3d}) and valence band maximum, VBM (E^{Ge}_{VBM}) of (111)Ge film; (b) Al 2p core level (E^{Al}_{Al2p}) spectrum and VBM (E^{Al}_{VBM}) of 10 nm Al_2O_3 film, respectively.

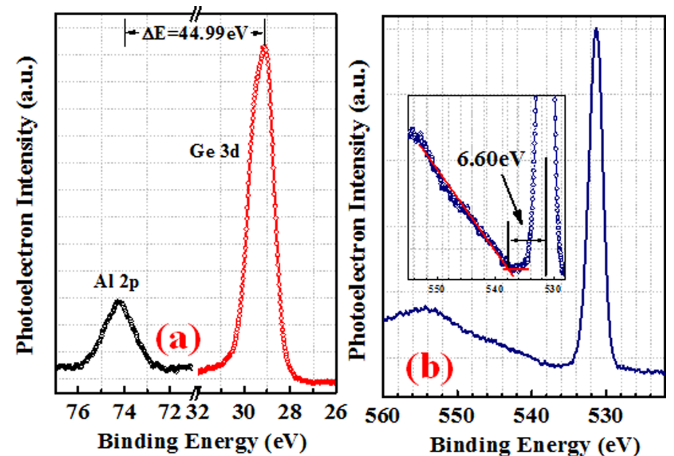

FIG. 11. XPS spectra of (a) Ge 3d (E^{Ge}_{Ge3d}) and Al 2p core level (E^{Al}_{Al2p}) spectra of 1 nm thin Al_2O_3 film/(111)Ge interface, and (b) the CL spectrum of 10 nm Al_2O_3 film. The band gap of Al_2O_3 was determined to be 6.6 ± 0.05 eV.

epilayer, our results achieved a valence band offset relation of $\Delta E_V(110)\text{Ge} > \Delta E_V(100)\text{Ge} \geq \Delta E_V(111)\text{Ge}$ and conduction band offset of $\Delta E_c(111)\text{Ge} > \Delta E_c(110)\text{Ge} > \Delta E_c(100)\text{Ge}$ after careful investigation of XPS results on Al_2O_3/Ge heterointerface. The result obtained from this analysis is also presented in Table IV. One can find that the

TABLE III. Core-level to VBM binding-energy difference for Al_2O_3 and epitaxial (111)Ge grown on (111)A GaAs substrate.

Material and interface	Binding energy difference	Measured band offsets of Al_2O_3/(111)Ge	
		ΔE_V (eV)	ΔE_C (eV)
Ge	$E^{Ge}_{Ge3d} - E^{Ge}_{VBM} = 29.58 \pm 0.05$ eV		
10 nm Al_2O_3	$E^{Al}_{Al2p} - E^{Al}_{VBM} = 71.47 \pm 0.05$ eV		
1 nm Al_2O_3 on Ge	$E^{Al}_{Al2p} - E^{Ge}_{Ge3d} = 44.99$ eV		
E_g of Al_2O_3	6.60 ± 0.05 eV	3.10 ± 0.05	2.83 ± 0.1

TABLE IV. Band offset values of Al_2O_3 on crystallographic oriented epitaxial Ge layers.

	(100)	(110)	(111)A
ΔE_V (eV)	3.17 ± 0.05	3.34 ± 0.05	3.10 ± 0.05
ΔE_C (eV)	2.66 ± 0.1	2.50 ± 0.1	2.83 ± 0.1
E_g of Al_2O_3 (eV)	6.5 ± 0.05	6.51 ± 0.05	6.6 ± 0.05

crystallographic orientation of Ge epilayer has a strong influence on the band offset properties, which is believed to be the quality of the Ge/GaAs heterojunction growth, the surface reconstruction of Ge and the interface quality at the Al_2O_3/Ge heterointerface. Figure 12 shows the band alignment diagram of the measured Al_2O_3 on (a) (100)Ge, (b) (110)Ge, and (c) (111)Ge heterointerface, respectively. The band offset values of Ge on (100), (110), and (111)A GaAs substrates are included in this figure from Ref. 40. From this result, one can find that the ΔE_v and ΔE_c of Al_2O_3 on crystallographic oriented Ge epilayers are well above 1 eV, as needed for blocking electrons and holes[38] for carrier transport in the fabricated Ge MOSFETs. Although the transport properties also strongly depends on the interface states between the high-κ and the Ge layer, there is no reliable energy gap data of GeO_x ($1 \leq x \leq 2$) available due to ultra-thin and nonstoichiometric interfacial compound. Therefore, the only measured band alignment of Al_2O_3 on crystallographic oriented epitaxial Ge is included in Fig. 12. Figure 13 shows the histogram of ΔE_v and ΔE_c distribution obtained from ALD Al_2O_3 oxide film on epitaxial crystallographic oriented Ge layers. Thus, the measured band offset values on crystallographic oriented epitaxial Ge can provide a promising path for Ge based transistor design.

IV. CONCLUSIONS

In conclusion, we have shown that sharp interface quality of the epitaxial Ge/GaAs heterostructures can be grown *in-situ* on (100), (110), and (111)A GaAs substrates using two separate molecular beam epitaxy chambers, as confirmed by x-ray diffraction and cross-sectional TEM microscopy. The band alignment properties of Al_2O_3 on epitaxial crystallographic oriented Ge were investigated using x-ray photoelectron spectroscopy. Valence band offsets of 3.17 eV, 3.34 eV, and 3.10 eV have been derived from XPS data on Al_2O_3/(100)Ge, Al_2O_3/(110)Ge, and

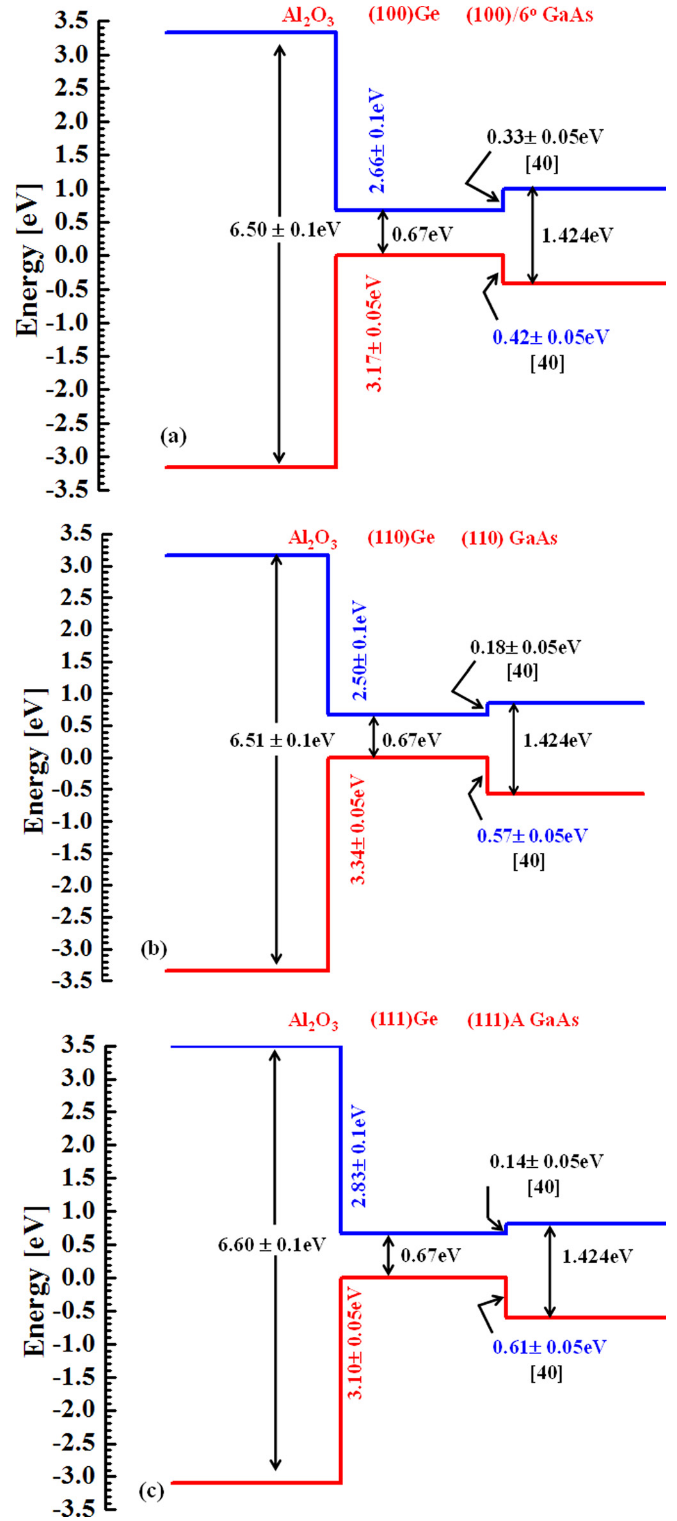

FIG. 12. Energy-band diagram of the Al_2O_3/Ge heterojunction obtained from XPS measurements on (a) (100)Ge, (b) (110)Ge, and (c) (111)Ge, respectively. The conduction band discontinuity, ΔE_c has been calculated based on the measured ΔE_v and the difference in bandgap of Al_2O_3 and Ge, where $\Delta E_g = \Delta E_v + \Delta E_c$. The Ge/GaAs band offset in each orientation is included from Ref. 40.

Al_2O_3/(111)Ge heterointerfaces, respectively. Using XPS data, variations in ΔE_v related to the Ge crystallographic orientation is $\Delta E_V(110)\text{Ge} > \Delta E_V(100)\text{Ge} \geq \Delta E_V(111)\text{Ge}$. Moreover, the ΔE_c is related to the crystallographic orientations as $\Delta E_c(111)\text{Ge} > \Delta E_C(110)\text{Ge} > \Delta E_c(100)\text{Ge}$ using

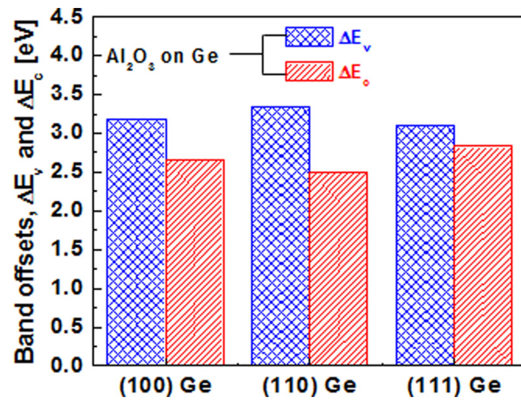

FIG. 13. Histogram of band offset distribution obtained from Al_2O_3/Ge heterointerface on crystallographic oriented Ge layers. The highest ΔE_v value was obtained on (110)Ge.

the measured bandgap of Al_2O_3 in each orientation and with the Ge bandgap of 0.67 eV. The high-quality heterointerface and the band offset parameters for carrier confinement can offer a promising virtual substrate technology integrated on Si substrate for extending the performance and application of Ge-based p-and n-channel metal-oxide field effect transistor design.

[1]International Technology Roadmap for Semiconductors (ITRS), 2011 edition, Process Integration, Devices, and Structures (PIDS), Chapter (2011).
[2]M. Radosavljevic, B. Chu-Kung, S. Corcoran, M. K. Hudait, G. Dewey, J. M. Fastenau, J. Kavalieros, W. K. Liu, D. Lubyshev, M. Metz, K. Millard, W. Rachmady, U. Shah, and R. Chau, *in IEEE Conference Proceedings of International Electron Devices Meeting (IEDM)* (IEEE, New York, 2009), p. 319.
[3]Y. Sun, in *International Symposium on VLSI Technology, Systems, and Applications* (IEEE, New York, 2010), p. 149.
[4]A. Ali, H. Madan, M. J. Barth, M. J. Hollander, J. B. Boos, B. R. Bennett, and S. Datta, in *International Symposium on VLSI Technology, Systems, and Applications* (IEEE, New York, 2012), p. 181.
[5]M. K. Hudait, ECS Trans. **45**, 581 (2012).
[6]M. K. Hudait, G. Dewey, S. Datta, J. M. Fastenau, J. Kavalieros, W. K. Liu, D. Lubyshev, R. Pillarisetty, W. Rachmady, M. Radosavljevic, T. Rakshit, and R. Chau, in *IEEE Conference Proceedings of International Electron Devices Meeting (IEDM)* (IEEE, New York, 2007), p. 625.
[7]L. Ming, L. Haiou, T. Chak Wah, and L. Kei May, IEEE Electron Device Lett. **33**, 498 (2012).
[8]M. Radosavljevic, T. Ashley, A. Andreev, S. D. Coomber, G. Dewey, M. T. Emeny, M. Fearn, D. G. Hayes, K. P. Hilton, M. K. Hudait, R. Jefferies, T. Martin, R. Pillarisetty, W. Rachmady, T. Rakshit, S. J. Smith, M. J. Uren, D. J. Wallis, P. J. Wilding, and R. Chau, in *IEEE Conference Proceedings of International Electron Devices Meeting (IEDM)* (IEEE, New York, 2008), p. 727.
[9]R. Pillarisetty, B. Chu-Kung, S. Corcoran, G. Dewey, J. Kavalieros, H. Kennel, R. Kotlyar, V. Le, D. Lionberger, M. Metz, N. Mukherjee, J. Nah, W. Rachmady, M. Radosavljevic, U. Shah, S. Taft, H. Then, N. Zelick, and R. Chau, in *IEEE Conference Proceedings of International Electron Devices Meeting (IEDM)* (IEEE, New York, 2010), p. 150.
[10]J. B. Boos, B. R. Bennett, N. A. Papanicolaou, M. G. Ancona, J. G. Champlain, Y. C. Chou, M. D. Lange, J. M. Yang, R. Bass, D. Park, and B. V. Shanabrook, IEICE Trans. Electron. **E91-C**, 1050 (2008).
[11]Y. Sun, S. E. Thompson, and T. Nishida, *Strain Effect in Semiconductors: Theory and Device Applications*, 1st ed. (Springer, 2009).
[12]M. V. Fischetti and S. E. Laux, J. Appl. Phys. **80**, 2234 (1996).
[13]J. Kim and M. V. Fischetti, J. Appl. Phys. **108**, 013710 (2010).
[14]Y. Sun, S. E. Thompson, and T. Nishida, J. Appl. Phys. **101**, 104503 (2007).
[15]M. L. Lee, E. A. Fitzgerald, M. T. Bulsara, M. T. Currie, and A. Lochtefeld, J. Appl. Phys. **97**, 011101 (2005).
[16]B.-F. Hsieh and S.-T. Chang, Solid-State Electron. **60**, 37 (2011).
[17]M. Radosavljevic, G. Dewey, D. Basu, J. Boardman, B. Chu-Kung, J. M. Fastenau, S. Kabehie, J. Kavalieros, V. Le, W. K. Liu, D. Lubyshev, M. Metz, K. Millard, N. Mukherjee, L. Pan, R. Pillarisetty, W. Rachmady, U. Shah, H. W. Then, and R. Chau, in *IEEE Conference Proceedings of International Electron Devices Meeting (IEDM)* (IEEE, New York, 2011), p. 765.
[18]Y. J. Yang, W. S. Ho, C. F. Haung, S. T. Chang, and C. W. Liu, Appl. Phys. Lett. **91**, 102103 (2007).
[19]S. Dissanayake, Y. Zhao, S. Sugahara, M. Takenaka, and S. Takaghi, J. Appl. Phys. **109**, 033709 (2011).
[20]T. Low, M. F. Li, G. Samudra, Y. Yeo, C. Zhu, A. Chin, and D. Kwong, IEEE Trans. Electron. Devices **52**, 2430 (2005).
[21]T. Krishnamohan, D. Kim, T. V. Dinh, A. Pham, B. Meinerzhagen, C. Jungemann, and K. Saraswat, in *IEEE Conference Proceedings of International Electron Devices Meeting (IEDM)* (IEEE, New York, 2008), p. 899.
[22]S. Dissanayake, K. Tomiyama, S. Sugahara, M. Takenaka, and S. Takagi, Appl. Phys. Express **3**, 041302 (2010).
[23]S. Nakaharai, T. Tezuka, N. Sugiyama, Y. Moriyama, and S. Takagi, Appl. Phys. Lett. **83**, 3516 (2003).
[24]C. H. Lee, T. Nishimura, N. Saido, K. Nagashio, K. Kita, A. Toriumi, in *IEEE Conference Proceedings of International Electron Devices Meeting (IEDM)* (IEEE, New York, 2009), p. 457.
[25]A. Toriumi, K. Kita, M. Toyama and H. Nomura, in *Advanced Gate Stacks for High-Mobility Semiconductors*, edited by A. Dimoulas, E. Gusev, P. C. McIntyre, and M. Heyns (Springer, Berlin, 2007).
[26]J. H. Choi, Y. Mao, and J. P. Chang, Mater. Sci. Eng. R. **72**, 97 (2011).
[27]M. Perego, G. Seguini, and M. Fanciulli, J. Appl. Phys. **100**, 093718 (2006).
[28]S. J. Wang, A. C. H. Huan, Y. L. Foo, J. W. Chai, J. S. Pan, Q. Li, Y. F. Dong, Y. P. Feng, and C. K. Ong, Appl. Phys. Lett. **85**, 4418 (2004).
[29]H. Seo, F. Bellenger, K. B. Chung, M. Houssa, M. Meuris, M. Heyns, and G. Lucovsky, J. Appl. Phys. **106**, 044909 (2009).
[30]S. Swaminathan, Y. Sun, P. Pianetta, and P. C. McIntyre, J. Appl. Phys. **110**, 094105 (2011).
[31]S. Y. Chiam, W. K. Chim, C. Pi, A. C. H. Huan, S. J. Wang, J. S. Pan, S. Turner, and J. Zhang, J. Appl. Phys. **103**, 083702 (2008).
[32]M. Perego, G. Seguini, G. Scarel, and M. Fanciulli, Surf. Interface. Anal. **38**, 494 (2006).
[33]M. S. Rahman, E. K. Evangelou, A. Dimoulas, G. Mavrou, and S. Galata, J. Appl. Phys. **103**, 064514 (2008).
[34]M. S. Rahman, E. K. Evangelou, N. Konofaos, and A. Dimoulas, J. Appl. Phys. **112**, 094501 (2012).
[35]H. Shang, H. Okorn-Schimdt, J. Ott, P. Kozlowski, E. C. Jones, H.-S. P. Wong, and W. Hanesch, IEEE Electron Device Lett. **24**, 242 (2003).
[36]W. E. Spicer, I. Lindau, P. Skeath, C. Y. Su, and P. Chye, Phys. Rev. Lett. **44**, 420 (1980).
[37]P. Chiaradia, M. Fanfoni, P. Nataletti, P. De Padova, L. J. Brillson, M. L. Slade, R. E. Viturro, D. Kilday, and G. Margaritondo, Phys. Rev. B **39**, 5128 (1989).
[38]J. Robertson and B. Falabretti, J. Appl. Phys. **100**, 014111 (2006).
[39]M. K. Hudait, Y. Zhu, N Jain, S. Vijayaraghavan, A. Saha, T. Merritt, and G. A. Khodaparast, J. Vac. Sci. Technol. B **30**, 051205(2012).
[40]M. K. Hudait, Y. Zhu, N. Jain, and J. L. Hunter, Jr., J. Vac. Sci. Technol. B **31**, 011206 (2013).
[41]E. A. Kraut, R. W. Grant, J. R. Waldrop, and S. P. Kowalczyk, Phys. Rev. Lett. **44**, 1620 (1980).
[42]S. J. Lee, C. Zhu and D. L. Kwong, in *Advanced Gate Stacks for High-Mobility Semiconductors*, edited by A. Dimoulas, E. Gusev, P. C. McIntyre, and M. Heyns (Springer, Berlin, 2007).
[43]A. Dimoulas, E. Gusev, P. C. McIntyre, and M. Heyns, *Advanced Gate Stacks for High-Mobility Semiconductors* (Springer, Berlin, 2007).
[44]L. J. Brillson, *Surfaces and Interfaces of Electronic Materials* (Wiley-VCH, Germany, 2010).
[45]C. Jia, Y. Chen, Y. Guo, X. Liu, S. Yang, W. Zhang, and Z. Wang, Nanoscale Res. Lett. **6**, 316 (2011).
[46]S. A. Chambers, T. Droubay, T. C. Kaspar, and M. Gutowski, J. Vac. Sci. Technol. B **22**, 2205 (2004).